AGU PUBLICATIONS

Geophysical Research Letters

RESEARCH LETTER

10.1002/2016GL070111

Key Points:

- Sea spray geoengineering changed regional ocean net primary productivity (NPP) significantly (± ~700 mg C m^{-2} d^{-1}) in model simulations
- Changes in NPP were mainly caused by lower temperatures in the geoengineering run than in the control run instead of lower available light
- The geoengineering run had lower ocean carbon uptake than the control run (difference up to 0.08 Gt C yr^{-1}) in a low-CO_2 emission scenario

Supporting Information:

- Supporting Information S1

Correspondence to:
A.-I. Partanen,
antti-ilari.partanen@concordia.ca

Citation:
Partanen, A.-I., D. P. Keller, H. Korhonen, and H. D. Matthews (2016), Impacts of sea spray geoengineering on ocean biogeochemistry, *Geophys. Res. Lett.*, *43*, 7600–7608, doi:10.1002/2016GL070111.

Received 14 MAR 2016
Accepted 2 JUL 2016
Accepted article online 6 JUL 2016
Published online 22 JUL 2016

Impacts of sea spray geoengineering on ocean biogeochemistry

Antti-Ilari Partanen[1,2], David P. Keller[3], Hannele Korhonen[2], and H. Damon Matthews[1]

[1]Department of Geography, Planning and Environment, Concordia University, Montreal, Quebec, Canada, [2]Climate Change, Finnish Meteorological Institute, Helsinki, Finland, [3]Helmholtz Centre for Ocean Research Kiel (GEOMAR), Kiel, Germany

Abstract We used an Earth system model of intermediate complexity to study the effects of Solar Radiation Management (SRM) by sea spray geoengineering on ocean biogeochemistry. SRM slightly decreased global ocean net primary productivity (NPP) relative to the control run. The lower temperatures in the SRM run decreased NPP directly but also indirectly increased NPP in some regions due to changes in nutrient availability resulting from changes in ocean stratification and circulation. Reduced light availability had a minor effect on global total NPP but a major regional effect near the nutrient-rich upwelling region off the coast of Peru, where light availability is the main limiting factor for phytoplankton growth in our model. Unused nutrients from regions with decreased NPP also fueled NPP elsewhere. In the context of RCP4.5 simulation used here, SRM decreased ocean carbon uptake due to changes in atmospheric CO_2 concentrations, seawater chemistry, NPP, temperature, and ocean circulation.

1. Introduction

A fear that global efforts to reduce greenhouse gas emissions might come too late to avoid dangerous climate impacts has stemmed ideas of cooling the climate deliberately by reducing the incoming solar radiation [*Crutzen*, 2006]. One of these ideas for Solar Radiation Management (SRM) is to inject sea spray particles into marine clouds to enhance their reflectivity [*Latham*, 1990; *Korhonen et al.*, 2010; *Latham et al.*, 2012] and also scatter solar radiation directly by the particles [*Partanen et al.*, 2012]. This technique is commonly known as marine cloud brightening or sea spray geoengineering.

Modeling studies suggest that SRM could help to bring the climate closer to preindustrial conditions in terms of temperature and precipitation [*Shepherd et al.*, 2009]. SRM could also affect the carbon cycle by increasing the carbon uptake of land and ocean in scenarios with continued high CO_2 emissions [*Matthews and Caldeira*, 2007; *Keller et al.*, 2014; *Tjiputra et al.*, 2015].

However, many studies have also highlighted the risks of SRM. On a global average, it would reduce rainfall [*Schmidt et al.*, 2012; *Alterskjaer et al.*, 2013], and regional changes could be detrimental [*Robock et al.*, 2008; *Irvine et al.*, 2010]. SRM has been proposed as a potential tool to remedy local climate impacts such as preserving coral reefs [*Latham et al.*, 2013] or preserving Arctic sea ice [*Rasch et al.*, 2009], but it could also pose risks to biological systems [*Russell et al.*, 2012].

Sea spray geoengineering, in particular, would likely have its own set of potential risks for ocean ecosystems. For example, by reducing the amount of available light and ocean temperature, sea spray geoengineering might alter the carbon uptake of the oceans directly by changing seawater chemistry and indirectly by changing phytoplankton production. Consequently, this could affect other biogeochemical cycles and ecology (e.g., food webs and fisheries). *Hardman-Mountford et al.* [2013] used a one-dimensional water column model to study the effect of reduced light availability on phytoplankton growth. Their results imply that even a significant reduction (90%) of solar radiation barely affects total column biological productivity but can alter considerably vertical distribution of productivity. However, their study did not consider how other processes, such as local cooling or horizontal transport of nutrients, would affect the marine ecosystems. Their model setup was also unable to capture broader effects on the ocean carbon cycle.

In this study, we used an Earth system model of intermediate complexity to model the effects of sea spray geoengineering on ocean biogeochemistry. Our main goal is to quantify the effects on ocean net primary productivity (NPP) and ocean carbon uptake. In addition, we aim to assess the relative importance of reduced light availability and ocean cooling, and to study the reversibility of the SRM-caused changes if SRM is terminated.

2. Methods

2.1. Modeling Approach

We used the version 2.9 of the University of Victoria Earth System Climate Model (UVic ESCM) [*Weaver et al*., 2001; *Eby et al*., 2013] to simulate the response of ocean biogeochemistry to sea spray geoengineering. The UVic ESCM is an Earth system model of intermediate complexity. It consists of a three-dimensional ocean circulation model, a terrestrial model, and a simple atmospheric energy-moisture balance model. The atmospheric CO_2 concentration is calculated interactively as a function of prescribed emissions and simulated carbon sinks allowing interaction between ocean and land carbon cycles. The circulation of the one-layer atmosphere is prescribed based on monthly climatological wind speed data created from 40 years of reanalysis data [*Kalnay et al*., 1996]. The ocean model has 19 vertical layers and includes a sea ice model and an improved version of the ocean biogeochemistry module [*Keller et al*., 2012] (see Text S1 in the supporting information for details). The biogeochemistry module includes two phytoplankton classes (nitrogen fixers and nonnitrogen fixers), zooplankton, particulate detritus, nitrate, oxygen, phosphate, dissolved inorganic carbon, and total alkalinity. The effects of iron limitation on marine primary productivity are also included using a dissolved iron masking approach. Air-sea gas exchange and ocean carbon chemistry follow the protocols from the Ocean Carbon-Cycle Model Intercomparison Project (OCMIP) [*Orr et al*., 1999]. The model has been used in several ocean biogeochemical studies and its skill at simulating the present-day ocean was assessed by *Keller et al*. [2012] (see also Text S1).

We modeled the radiative effects of SRM by prescribing radiative forcing taken from earlier sea spray geoengineering simulations [*Partanen et al*., 2012] with the aerosol-climate model ECHAM5.5-HAM2 [*Zhang et al*., 2012]. The SRM forcing was applied over three marine stratocumulus regions off the west coasts of North America, South America, and Southern Africa (Figure 1a). The annual global mean forcing was $-1\,W\,m^{-2}$, though locally, the monthly forcing was between around $-10\,W\,m^{-2}$ and $-100\,W\,m^{-2}$. The forcing included both direct and indirect aerosol radiative effects. The mean was calculated for each month of a year from 10 year model runs and interpolated onto the UVic ESCM grid. Thus, there was no interannual variability in the applied forcing. We used the Top-Of-the-Atmosphere (TOA) effective radiative forcing to modify the shortwave fluxes at the surface and the longwave surface fluxes at the TOA in the UVic ESCM. For more details about the forcing, see Text S2.

2.2. Experiment Design

All the runs with the UVic ESCM were started after a 10,000 year spin-up period under a fixed atmospheric CO_2 concentration and a historical simulation from 1750 to 2005. Historical simulations for different model setups were forced with historical CO_2 emissions. Forcing from anthropogenic sulfate aerosols was prescribed as increased surface albedo [*Matthews et al*., 2004; *Matthews and Zickfeld*, 2012] and forcing of non-CO_2 gases was applied transiently according to historical data. Other forcings (land-use change, solar, and volcanic aerosols) were set to their preindustrial values. From 2005 to 2100, we prescribed CO_2 emissions consistent with the RCP4.5 scenario [*Thomson et al*., 2011]. Forcings from other greenhouse gases and sulfate aerosols were also prescribed according to the RCP4.5 scenario.

The full list of simulations is given in Table 1. Our control simulation (CTRL) was a standard RCP4.5 simulation without SRM from year 2005 to 2100. In our baseline SRM simulation GEO, SRM started in the year 2020 and continued throughout the simulation until 2100. To test the reversibility of ocean biogeochemistry to the SRM perturbation, we conducted an experiment GEO-STOP, where SRM was ended after 20 years of deployment. Furthermore, to study the relative effects of reduced light availability and ocean cooling we conducted two additional experiments. In GEO-COOLING, SRM was allowed to affect only temperature, while the ocean biogeochemistry module was given unmodified radiative fluxes. Correspondingly, in the simulation GEO-SHADING, SRM affected only the radiative fluxes given to the biogeochemistry module, but did not directly affect the temperature (i.e., only light-reducing effects were included).

To further study the relative contributions of reduced light availability and ocean temperature changes on ocean biogeochemistry, we conducted another set of experiments where ocean biogeochemical rate coefficients (e.g., for phytoplankton growth) were temperature independent [*Taucher and Oschlies*, 2011]. These experiments can be used to help infer whether changes in NPP are due to physical or biological drivers. In

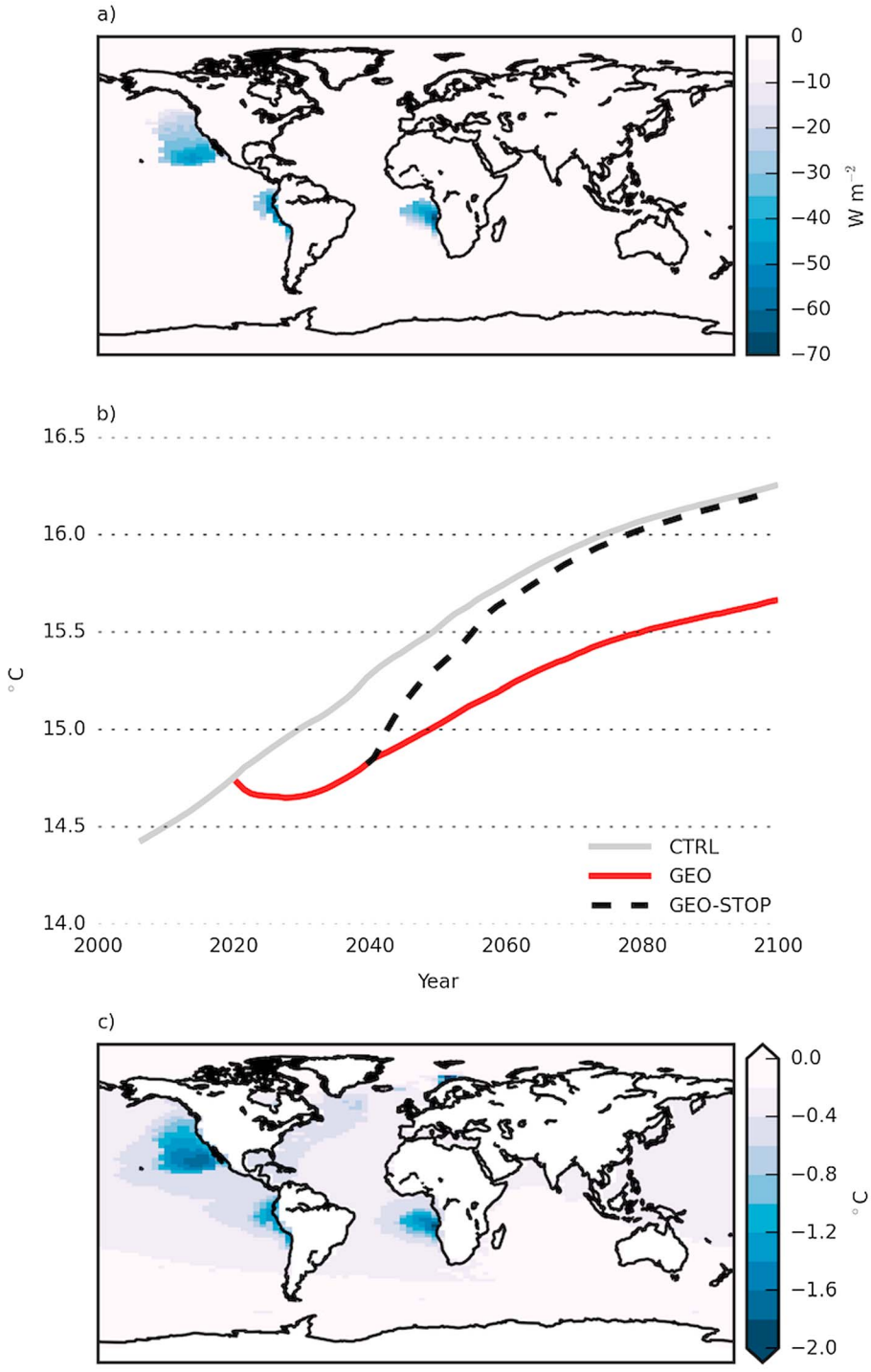

Figure 1. (a) Annual mean effective radiative forcing from SRM, including shortwave and longwave contributions. (b) Annual global mean atmospheric surface temperature. (c) The difference in ocean potential temperature of the uppermost layer (down to 50 m) between GEO and CTRL at year 2030.

all other ways these experiments were identical to the ones described above and are named with a suffix NOTEMP added to the end of the simulation name (e.g., CTRL_NOTEMP, see Table 1).

Finally, we did a sensitivity simulation GEO-CO2-CONC with CO_2 concentration prescribed to follow that in CTRL. In other respects, this simulation was identical to GEO. This simulation helps to disentangle direct effects of SRM on the ocean carbon cycle from the indirect effects of changed atmospheric CO_2 concentration.

Table 1. Description of the Model Experiments

Experiment	Description
	With Temperature-Dependent Ocean Biogeochemical Rate Coefficients
CTRL	Control simulation based on RCP4.5 scenario.
GEO	As CTRL, but geoengineering started in 2020.
GEO-STOP	As GEO, but geoengineering was shut down after 20 years.
GEO-COOLING	As GEO, but geoengineering affected only by cooling.
GEO-SHADING	As GEO, but geoengineering affected only the solar radiation available for phytoplankton growth.
GEO-CO2-CONC	As GEO, but atmospheric CO_2 concentration was prescribed to follow that in CTRL.
	With Temperature-Independent Ocean Biogeochemical Rate Coefficients
CTRL_NOTEMP	Control simulation based on RCP4.5 scenario. Rate coefficients for marine biogeochemistry were independent of temperature.
GEO_NOTEMP	As CTRL_NOTEMP, but geoengineering started in 2020.
GEO-STOP_NOTEMP	As GEO_NOTEMP, but geoengineering was shut down after 20 years.
GEO-COOLING_NOTEMP	As GEO_NOTEMP, but geoengineering affected only by cooling.
GEO-SHADING_NOTEMP	As GEO_NOTEMP, but geoengineering affected only the solar radiation available for phytoplankton growth.

3. Results and Discussion

3.1. Global Temperature Response

The evolution of global mean surface air temperature is shown in Figure 1b. In CTRL, temperature increased from 14.4°C in the year 2005 to 16.3°C in the year 2100. SRM in the simulation GEO lowered temperature below that of CTRL by about 0.4°C during the first two decades of SRM and by 0.6°C by 2100. When SRM was stopped in 2040 (GEO-STOP), temperature increased rapidly within a few decades and asymptotically approached temperature in CTRL. This termination effect was similar to results presented in many previous studies [*Matthews and Caldeira*, 2007; *Brovkin et al*., 2008; *Ross and Matthews*, 2009; *Jones et al*., 2013]. Due to negligible temperature differences between GEO-SHADING and CTRL, and between GEO-COOLING and GEO, only CTRL, GEO, and GEO-STOP are shown in Figure 1b.

The difference in ocean potential temperature in the uppermost layer between GEO and CTRL was strongly localized (Figures 1c and S1). In the SRM regions in the year 2030, the difference was about −2°C but was smaller than −0.6°C outside these regions.

3.2. Effects on the Ocean Net Primary Productivity

Both climate change and SRM caused changes in NPP. In CTRL, NPP decreased steadily through the 21st century (Figure 2a). The average global total ocean NPP in 2090–2099 (48.8 Gt C yr^{-1}) was 3.2% lower than that in 1990–1999. This decrease was very close to the multimodel-mean value of −3.6% for the same time period in the Coupled Model Intercomparison Project Phase 5 (CMIP5) simulations [*Bopp et al*., 2013]. SRM slightly reduced NPP further in GEO relative to CTRL (Figure 2a). In 2030 (after 10 years of SRM), NPP in GEO was 0.43 Gt C yr^{-1} (0.9%) lower than in CTRL. When viewed as a global integral the effects of SRM on NPP appear to be transient, with the strong effects early on (2030) and almost no difference by the end of the simulations. However, when viewed regionally (see below) significant differences in NPP are evident throughout the simulation.

Figure 3a shows the annual mean NPP in CTRL for year 2030. Of the three SRM regions (inside blue lines in Figure 3), only the one off the coast of Peru overlapped strongly with a region of high NPP (about 250–1750 mg C m^{-2} d^{-1}). NPP in the other two regions was mostly below 250 mg C m^{-2} d^{-1}.

The difference in NPP in 2030 between GEO and CTRL is displayed in Figure 3b. The largest effects occurred in the Eastern Pacific inside the SRM regions. The largest decrease was in the upwelling region off the coast of Peru (−503 mg C m^{-2} d^{-1} (−27%)). The largest increase was 312 mg C m^{-2} d^{-1} (84%). The SRM-induced changes in NPP between the two SRM regions in the Eastern Pacific (an area of high NPP in CTRL) were mainly negative. Areas with negative SRM-induced changes in NPP were consistently near areas with positive SRM-induced changes in NPP, suggesting that nutrients were transported from regions with reduced NPP to fuel NPP elsewhere. For example, just south of the region with largest decrease in NPP, there was positive change because unused nutrients were transported into this normally nutrient-limited region (Figure S2). The cancelation of regional positive and negative NPP changes means that the relatively small

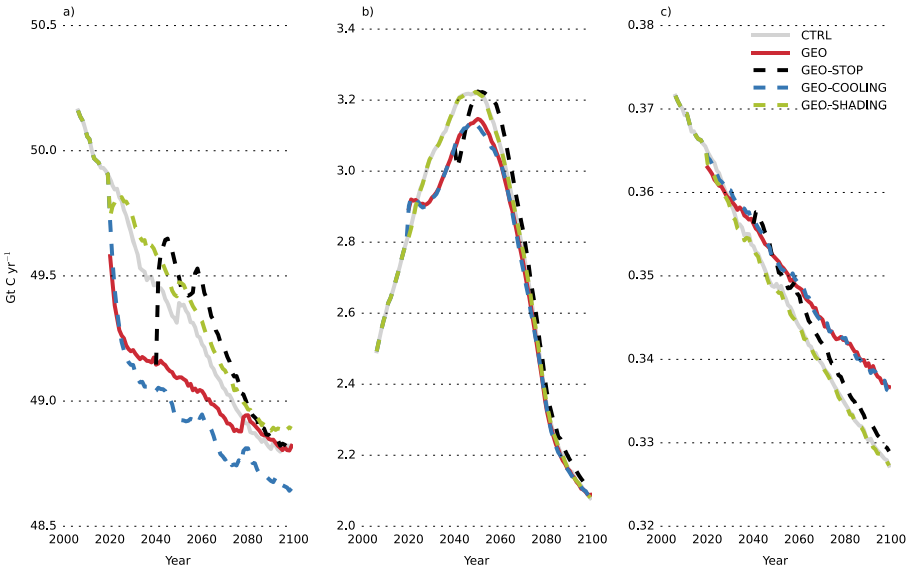

Figure 2. (a) Global total ocean net primary productivity. (b) Total carbon flux from atmosphere to ocean. (c) Global total export production at 2.2 km. Note the truncated *y* scale in the graphs.

global total NPP change from SRM (Figure 2a) should be interpreted with caution, as it does not reflect these potentially large regional changes.

Both the negative and positive regional differences grew stronger by 2100 (Figure S3b). The larger decrease in the SRM regions was caused by larger temperature difference between GEO and CTRL (Figure S1), and positive increases were caused by transport of nutrients which reached farther regions by 2100, and fueled NPP even in the high-NPP region in the Indian Ocean (Figures S3a and S3b). Over time, the regional NPP increase compensated for the decreased NPP near the SRM regions and the global total NPP approached that of CTRL (Figure 2a). Consequently, the difference in global total NPP between GEO and CTRL was only −0.01 Gt C yr^{-1} (−0.03%) in 2100.

The sensitivity simulations (GEO-COOLING and GEO-SHADING, and simulations with temperature-independent ocean biogeochemical rate coefficients) help to understand the mechanisms that led to the simulated NPP changes. From Figure 2a it can be seen that NPP in GEO-COOLING evolved in a similar way as in GEO and that GEO-SHADING is quite close to CTRL. Therefore, the first-order conclusion is that the temperature difference between GEO and CTRL was the main cause of the change in NPP due to SRM, while reduced light availability had a smaller effect. However, there are important complications to this first-order result. In GEO-SHADING, NPP was reduced inside the SRM regions in a similar way as in GEO, although the effect was smaller (Figure 3c). The negative effect of SRM on NPP in GEO-SHADING did not extend outside the SRM regions as in GEO (Figure 3b) or in GEO-COOLING (Figure S4). There was a similar region of positive NPP change in the Eastern Pacific in GEO-SHADING as in GEO, due to the transport of unused nutrients from the SRM region off the coast of Peru to fuel production elsewhere. The positive change in that region overcompensated for the decrease in NPP in the SRM region (Figure 3c) as the global total NPP was slightly higher in GEO-SHADING than in CTRL (Figure 2a). Thus, reduced light availability increased the global total NPP.

In the sensitivity runs with temperature-independent ocean biogeochemical rate coefficients, SRM increased global total NPP (Figure S5a), in contrast to the default runs. This suggests that indirect effects of the negative temperature difference between GEO and CTRL (i.e., increased nutrient availability due to changes in stratification and circulation) had a positive effect on global total NPP. However, this positive effect was smaller than the decrease in NPP due to direct temperature effects in GEO as NPP was lower in GEO compared to CTRL.

3.3. Effects on Ocean Carbon Cycle

Figure 2b shows the carbon flux from atmosphere to ocean in different simulations (see Figure S6 for spatial fluxes). During the first years of SRM, carbon uptake was higher in GEO than in CTRL, but for the rest of the simulation, GEO had lower carbon uptake by the oceans. This result was in contrast to previous studies where

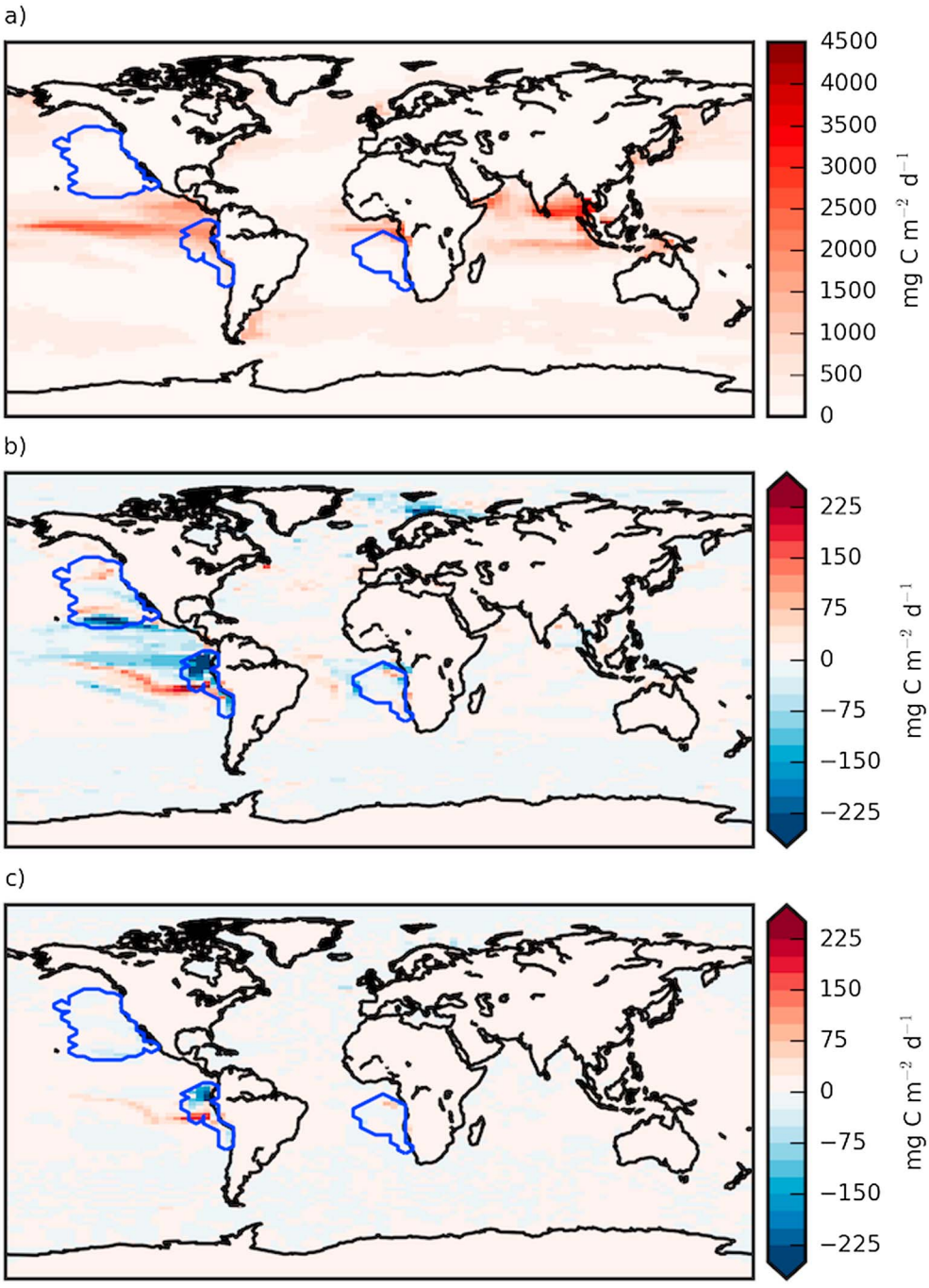

Figure 3. Vertically integrated mean ocean net primary productivity at year 2030 in (a) CTRL and difference from the CTRL in (b) GEO and (c) GEO-SHADING. The blue lines encircle the SRM regions.

SRM increased carbon uptake by oceans [*Matthews and Caldeira*, 2007; *Keller et al*., 2014; *Tjiputra et al*., 2015]. However, these studies were based on high CO_2 emission scenarios and more uniform forcing from SRM. When we reran the general solar dimming experiment (called SRM) by *Keller et al*. [2014] with emissions from RCP4.5 scenario instead of RCP8.5, the ocean carbon uptake was similar to the results presented here. Therefore, our results suggest that the decreased ocean carbon uptake due to SRM is not specific to the sea spray geoengineering technique or the geographically confined forcing, but is rather a general feature of low-emission scenarios.

Counterintuitively, one of the main reasons for the lower ocean carbon uptake in GEO is not because of the direct effect of SRM on the ocean, but rather because of how cooler air temperatures affected terrestrial carbon storage and consequently the atmospheric CO_2 concentration (pCO_2, Figure S7a) that controls ocean carbon uptake. In GEO, land carbon storage was 33 Gt C higher in 2100 than in CTRL as a result of the land carbon cycle response, which is regulated by direct temperature effects on photosynthesis and soil respiration [*Matthews et al*., 2005; *Keller et al*., 2014], to lower temperatures (Figures 1b and 1c). With higher land carbon storage, atmospheric CO_2 was lower in GEO (17 ppm CO_2 by 2100, Figure S7a). This difference led to a lower atmosphere-ocean pCO_2 gradient (0.8 ppm by 2100, Figure S7b) in GEO, which caused the ocean to take up less carbon, especially in the Southern Ocean. In CTRL, ocean total carbon in 2100 was 260 Gt C higher than in 2006 (37,348 Gt C) whereas the increase in GEO was only 256 Gt C. In the sensitivity simulation with prescribed atmospheric CO_2 concentrations (GEO-CO2-CONC), ocean carbon uptake was higher with SRM than in CTRL (Figure S8). This suggests that the direct effect of SRM would increase ocean carbon uptake if there were no carbon cycle feedbacks. Since the differences in ocean carbon content were driven mostly by pCO_2 differences, it is not surprising that changes in ocean carbon were almost entirely in the upper water column above 2000 m (Figure S9). However, there were significant spatial variation in the difference in ocean carbon storage between GEO and CTRL (Figure S10) that cannot be explained by pCO_2 differences alone. Ocean carbon content decreased first in the SRM regions (Figure S10a) and increased later in Indian Ocean, North Atlantic Ocean, and Arctic Ocean (Figure S10b).

These more direct and sometimes highly regional effects of SRM on ocean carbon cycling can be understood by looking at changes in the biological and solubility pumps. Changes in the biological pump can be investigated by looking at the export of organic matter out of the euphotic zone and into the deep ocean. Global total particulate organic carbon export at 130 m (Figure S11a) and 2.2 km depth (Figure 2c) were slightly higher in GEO than in CTRL with large regional variations that closely resemble the changes in NPP (Figures 3b and S1b). In many places the spatial changes in export appear to be correlated with the changes in the vertically integrated ocean carbon content (Figure S10). This suggests that changes in biological export were driving at least some of the ocean carbon content difference, something that was also generally found by *Tjiputra et al*. [2015].

SRM-related changes in the solubility pump (aside from the previously mentioned difference in pCO_2) can be investigated by looking at changes in ocean circulation, temperature, stratification, and buffering. Meridional overturning circulation, which decreased with climate change in all simulations, was higher in GEO than in CTRL (Figure S12). Stratification was also generally lower in GEO (Figure S13) because the upper ocean was cooler (Figure 1c). On longer time scales, stronger meridional overturning circulation can be expected to increase ocean carbon uptake [*Schmittner*, 2005]. A reduction in stratification and lower temperatures should also allow the mixed layer to more easily exchange, hold, and mix atmospheric CO_2 to deeper depths thereby enhancing ocean carbon uptake. However, by 2100, none of these effects were large enough to overcome the difference in pCO_2 that resulted in less carbon uptake. Since the solubility pump is driven by complex carbon chemistry we also investigated how the ocean's buffering capacity changed in response to SRM. The Revelle factor, which is inversely proportional to the oceans' capacity to absorb atmospheric CO_2 [*Sabine et al*., 2004], increased in all simulations with rising pCO_2 (acting as a strong positive feedback to the atmospheric pCO_2 by reducing the efficiency of ocean carbon uptake; not shown). Even with the pCO_2 difference between the simulations, the Revelle factor was noticeably higher in GEO, relative to CTRL, in the SRM regions (Figure S14), suggesting that SRM effects on ocean biogeochemistry reduced the efficiency of carbon uptake in these regions.

3.4. Reversibility of the Effects of SRM

As discussed in section 3.1, stopping SRM (GEO-STOP) led to a rapid rise of global mean temperature within a couple of decades. Directly after stoppage of SRM, NPP in GEO-STOP increased to a higher level than in CTRL (Figure 2a). The sharp increase was associated with a rapid recovery of NPP in the light-limited region off the coast of Peru and a much slower decrease in NPP within the following decades in the areas where NPP had increased due to SRM.

After the stoppage of SRM, terrestrial carbon uptake decreased with higher temperatures which increased atmospheric pCO_2 compared to GEO. Consequently, the carbon flux from the atmosphere to the ocean

(Figure 2b) in GEO-STOP increased above the level in CTRL by year 2050 before returning asymptotically. The ocean total carbon content was virtually the same in GEO-STOP and CTRL in the year 2100. Export production (Figures 2c and S8a) also slowly and asymptotically approached its respective trajectory in CTRL at both the global mean and regional level. Therefore, within the ecosystem represented in the UVic ESCM, the effects of SRM were reversible. However, the model does not take into account any harm done to fisheries or broader marine food webs. It is likely that the significant regional effects on NPP could cause changes in parts of the ecosystem that are not included in the model, and that some of these changes, such as species going extinct or migrating into other areas, might be irreversible.

4. Conclusions

We have shown here that sea spray geoengineering has the potential to cause substantial regional changes in ocean biogeochemistry. The magnitude of regional changes in NPP found here differed from the results of a previous study with a detailed column model that considered only light availability [*Hardman-Mountford et al*., 2013], neglecting changes in temperature, horizontal nutrient transport, and ocean circulation. Our sensitivity simulations that separated the effects of ocean cooling from effects of reduced light availability show that it was the changes in ocean temperature, including the indirect effects of nutrient availability due to circulation changes that accounted for most of the regional NPP changes. The main exception to this was near the coast of Peru, where light is the main limiting factor for phytoplankton growth in this model. Finally, in contrast to previous studies [*Matthews and Caldeira*, 2007; *Keller et al*., 2014; *Tjiputra et al*., 2015], SRM indirectly decreased the ocean carbon uptake in our simulations. It therefore appears that previous findings of enhanced ocean carbon uptake due to SRM do not necessarily hold in the context of slowly increasing, stable, or potentially decreasing atmospheric CO_2 concentrations.

In conclusion, our results indicate that effects of sea spray geoengineering on marine ecosystems could be significant especially locally and that the causal chain of the effects is more complex than just reduced light availability or direct temperature effects. Moreover, the significant local changes in NPP could potentially lead to drastic changes in fisheries and broader food webs not described by our model. Thus, more detailed studies of the topic are needed to fully understand the dynamics of sea spray geoengineering and marine ecosystems.

Acknowledgments
This work was supported by the Emil Aaltonen Foundation, the Academy of Finland (project 250348) and the European Research Council (646857-ECLAIR). The UVic ESCM model was run through Compute Canada network at supercomputer Guillimin of McGill University in Montreal, Canada. Code to calculate Revelle factor was based on the Matlab version of the CO2SYS program (doi: 10.3334/CDIAC/otg.CO2SYS_MATLAB_v1.1). Simulation and input data for this manuscript are available on request from the corresponding author (antti-ilari.partanen@concordia.ca).

References

Alterskjaer, K., J. E. Kristjánsson, O. Boucher, H. Muri, U. Niemeier, H. Schmidt, M. Schulz, and C. Timmreck (2013), Sea-salt injections into the low-latitude marine boundary layer: The transient response in three Earth system models, *J. Geophys. Res. Atmos.*, *118*, 12,195–12,206, doi:10.1002/2013JD020432.

Bopp, L., et al. (2013), Multiple stressors of ocean ecosystems in the 21st century: Projections with CMIP5 models, *Biogeosciences*, *10*(10), 6225–6245, doi:10.5194/bg-10-6225-2013.

Brovkin, V., V. Petoukhov, M. Claussen, E. Bauer, D. Archer, and C. Jaeger (2008), Geoengineering climate by stratospheric sulfur injections: Earth system vulnerability to technological failure, *Clim. Change*, *92*(3-4), 243–259, doi:10.1007/s10584-008-9490-1.

Crutzen, P. (2006), Albedo enhancement by stratospheric sulfur injections: A contribution to resolve a policy dilemma?, *Clim. Change*, *77*(3-4), 211–220, doi:10.1007/s10584-006-9101-y.

Eby, M., et al. (2013), Historical and idealized climate model experiments: An intercomparison of Earth system models of intermediate complexity, *Clim. Past*, *9*(3), 1111–1140, doi:10.5194/cp-9-1111-2013.

Hardman-Mountford, N. J., L. Polimene, T. Hirata, R. J. W. Brewin, and J. Aiken (2013), Impacts of light shading and nutrient enrichment geoengineering approaches on the productivity of a stratified, oligotrophic ocean ecosystem, *J. R. Soc. Interface*, *10*, 20130701, doi:10.1098/rsif.2013.0701.

Irvine, P. J., A. Ridgwell, and D. J. Lunt (2010), Assessing the regional disparities in geoengineering impacts, *Geophys. Res. Lett.*, *37*, L18702, doi:10.1029/2010GL044447.

Jones, A., et al. (2013), The impact of abrupt suspension of solar radiation management (termination effect) in experiment G2 of the Geoengineering Model Intercomparison Project (GeoMIP), *J. Geophys. Res. Atmos.*, *118*, 9743–9752, doi:10.1002/jgrd.50762.

Kalnay, E., et al. (1996), The NCEP/NCAR 40-year reanalysis project, *Bull. Am. Meteorol. Soc.*, *77*(3), 437–471, doi:10.1175/1520-0477(1996)077<0437:TNYRP>2.0.CO;2.

Keller, D. P., A. Oschlies, and M. Eby (2012), A new marine ecosystem model for the University of Victoria Earth system climate model, *Geosci. Model Dev.*, *5*(5), 1195–1220, doi:10.5194/gmd-5-1195-2012.

Keller, D. P., E. Y. Feng, and A. Oschlies (2014), Potential climate engineering effectiveness and side effects during a high carbon dioxide-emission scenario, *Nat. Commun.*, *5*, 3304, doi:10.1038/ncomms4304.

Korhonen, H., K. S. Carslaw, and S. Romakkaniemi (2010), Enhancement of marine cloud albedo via controlled sea spray injections: A global model study of the influence of emission rates, microphysics and transport, *Atmos. Chem. Phys.*, *10*(9), 4133–4143, doi:10.5194/acp-10-4133-2010.

Latham, J. (1990), Control of global warming?, *Nature*, *347*(6291), 339–340.

Latham, J., et al. (2012), Marine cloud brightening, *Philos. Trans. A. Math. Phys. Eng. Sci.*, *370*(1974), 4217–62, doi:10.1098/rsta.2012.0086.

Latham, J., J. Kleypas, R. Hauser, B. Parkes, and A. Gadian (2013), Can marine cloud brightening reduce coral bleaching?, *Atmos. Sci. Lett.*, *14*(4), 214–219, doi:10.1002/asl2.442.

Matthews, H., and K. Caldeira (2007), Transient climate–carbon simulations of planetary geoengineering, *Proc. Natl. Acad. Sci. U.S.A.*, *104*(24), 9949–9954, doi:10.1073/pnas.0700419104.
Matthews, H. D., and K. Zickfeld (2012), Climate response to zeroed emissions of greenhouse gases and aerosols, *Nat. Clim. Change*, *2*(5), 338–341, doi:10.1038/NCLIMATE1424.
Matthews, H. D., A. J. Weaver, K. J. Meissner, N. P. Gillett, and M. Eby (2004), Natural and anthropogenic climate change: Incorporating historical land cover change, vegetation dynamics and the global carbon cycle, *Clim. Dyn.*, *22*(5), 461–479, doi:10.1007/s00382-004-0392-2.
Matthews, H. D., M. Eby, A. J. Weaver, and B. J. Hawkins (2005), Primary productivity control of simulated carbon cycle-climate feedbacks, *Geophys. Res. Lett.*, *32*, L14708, doi:10.1029/2005GL022941.
Orr, J. C., R. G. Najjar, C. L. Sabine, and F. Joos (1999), Abiotic-HOWTO, Internal OCMIP Rep.
Partanen, A.-I., H. Kokkola, S. Romakkaniemi, V. M. Kerminen, K. E. J. Lehtinen, T. Bergman, A. Arola, and H. Korhonen (2012), Direct and indirect effects of sea spray geoengineering and the role of injected particle size, *J. Geophys. Res.*, *117*, D02203, doi:10.1029/2011JD016428.
Rasch, P. J., J. Latham, and C.-C. Chen (2009), Geoengineering by cloud seeding: Influence on sea ice and climate system, *Environ. Res. Lett.*, *4*, doi:10.1088/1748-9326/4/4/045112.
Robock, A., L. Oman, and G. L. Stenchikov (2008), Regional climate responses to geoengineering with tropical and Arctic SO_2 injections, *J. Geophys. Res.*, *113*, D16101, doi:10.1029/2008JD010050.
Ross, A., and D. H. Matthews (2009), Climate engineering and the risk of rapid climate change, *Environ. Res. Lett.*, *4*(4), 045103, doi:10.1088/1748-9326/4/4/045103.
Russell, L. M., et al. (2012), Ecosystem impacts of geoengineering: A review for developing a science plan, *Ambio*, *41*(4), 350–69, doi:10.1007/s13280-012-0258-5.
Sabine, C. L., et al. (2004), The oceanic sink for anthropogenic CO_2, *Science*, *305*(5682), 367–371, doi:10.1126/science.1097403.
Schmidt, H., et al. (2012), Solar irradiance reduction to counteract radiative forcing from a quadrupling of CO_2: Climate responses simulated by four Earth system models, *Earth Syst. Dyn.*, *3*(1), 63–78, doi:10.5194/esd-3-63-2012.
Schmittner, A. (2005), Decline of the marine ecosystem caused by a reduction in the Atlantic overturning circulation, *Nature*, *434*(7033), 628–633, doi:10.1038/nature03476.
Shepherd, J. G., et al. (2009), *Geoengineering the Climate: Science, Governance and Uncertainty*, Royal Soc., London.
Taucher, J., and A. Oschlies (2011), Can we predict the direction of marine primary production change under global warming?, *Geophys. Res. Lett.*, *38*, L02603, doi:10.1029/2010GL045934.
Thomson, A. M., et al. (2011), RCP4.5: A pathway for stabilization of radiative forcing by 2100, *Clim. Change*, *109*(1), 77–94, doi:10.1007/s10584-011-0151-4.
Tjiputra, J., A. Grini, and H. Lee (2015), Implication of future large-scale stratospheric aerosol injection on the land and ocean biogeochemistry, *J. Geophys. Res. Biogeosci.*, *120*, doi:10.1002/2015JG003045.
Weaver, A. J., et al. (2001), The UVic Earth system climate model: Model description, climatology, and applications to past, present and future climates, *Atmos. Ocean*, *39*(4), 361–428, doi:10.1080/07055900.2001.9649686.
Zhang, K., et al. (2012), The global aerosol-climate model ECHAM-HAM, version 2: Sensitivity to improvements in process representations, *Atmos. Chem. Phys.*, *12*(19), 8911–8949, doi:10.5194/acp-12-8911-2012.